Relativistic Band Structure of Gold*

C. B. SOMMERS† AND H. AMAR
Temple University, Philadelphia, Pennsylvania 19122
(Received 8 July 1969)

The electronic band structure of metallic gold has been calculated using a relativistic form of the Korringa-Kohn-Rostoker method, including a four-component spinor wave function and the full Dirac central-field Hamiltonian. The bands are compared with those of Schlosser's nonrelativistic calculation, using the same muffin-tin potential. The derived cross-sectional areas of the Fermi surface are in general agreement with Schoenberg's de Haas–van Alphen measurements. The allowed dipole transitions are used to interpret the optical measurements by Beaglehole. The peaks in the imaginary part of the dielectric constant being about 1 eV higher than our calculated band gaps, we conjecture that indirect transitions play an important role.

I. INTRODUCTION

IN the study of heavy elements, perturbation theory becomes inadequate for the treatment of relativistic effects such as spin-orbit coupling and mass-velocity and Darwin corrections.[1–3] To investigate the band structure of gold, we use the four-component Dirac Hamiltonian in conjunction with the Korringa-Kohn-Rostoker (KKR) or Green's-function method. Gold was chosen because of its large atomic number and its importance in completing our understanding of the properties of the noble metals and their alloys. The present authors and associates have previously calculated the band structures of several ordered and disordered IB-IIB alloys.[4]

In Sec. II we present the mathematical formalism based on the work of (KKR),[5] Ham and Segall (HS),[6] and Onodera.[7] In Sec. III we describe the actual calculation, the results found, and we compare the latter with the available de Haas–van Alphen and optical data.

II. THEORY

The relativistic formalism differs from the nonrelativistic KKR treatment in that the Schrödinger Hamiltonian inside the muffin-tin sphere is replaced by the Dirac central-field Hamiltonian. The wave function is then a four-component spinor. One generally constructs (at selected k points of the Brillouin zone) linear combinations of these wave functions belonging to the various irreducible representations of the crystallographic double-point groups, thus reducing appreciably the computational labor.

In order to simplify the physical problem, the crystal periodic potential is chosen to be spherically symmetric and of the muffin-tin form:

$$\begin{aligned} V(r)&=V_a(r)-V_0, && r<r_m \\ &=0, && r>r_m \end{aligned} \tag{1}$$

where $V_a(r)$ is the atomiclike potential centered about a particular lattice site, V_0 is the constant average potential between sites which has been subtracted from $V(r)$ for calculational purposes, and r_m is the muffin-tin radius which has been chosen to be one-half the nearest-neighbor distance. $V_a(r)$ has been calculated from a relativistic self-consistent atomic charge density, as supplied by Cromer,[8] coupled with a Lowdin-Alpha-type expansion[9] in spherical harmonics to include the effects of 14 nearest neighbors. The exchange term in the potential was calculated using a $\frac{2}{3}$ coefficient in front of the Slater $(\rho)^{1/3}$ approximation. This latter approximation was used for both the atomic as well as the crystal exchange effects.

We use the Dirac central-field Hamiltonian (in units of $m=c=\hbar=1$)

$$\mathcal{H}=\boldsymbol{\alpha}\cdot\mathbf{p}+\beta+V(r). \tag{2}$$

This Hamiltonian commutes with the total angular momentum J and the operator $K=\beta(\boldsymbol{\sigma}\cdot l+1)$. This lattice operator is particularly useful in that it specifies both J and l:

$$\begin{aligned} &K>0: J=l-\tfrac{1}{2}, \quad l=K, && \bar{l}=l-1; \\ &K<0: J=l+\tfrac{1}{2}, \quad l=-(K+1), && \bar{l}=l+1. \end{aligned} \tag{3}$$

The crystal eigenvalue problem can be written as

$$-(\boldsymbol{\alpha}\cdot\mathbf{p}+\beta-W)\psi(k,r)=V(r)\psi(k,r), \tag{4}$$

with $V(r)=V(r+R_n)$, where R_n is a lattice translation vector. The four-component spinor $\psi(k,r)$ must satisfy the Bloch condition

$$\psi(k,r+R_n)\equiv|\psi(r+R_n)\rangle_k=e^{i\mathbf{k}\cdot\mathbf{R}_n}|\psi(r)\rangle_k, \tag{5}$$

* Supported by the U. S. Atomic Energy Commission.
† This work is included in a thesis submitted by C. Sommers in partial fulfillment of the requirements of the Ph.D. degree at Temple University.
[1] L. E. Johnson, J. B. Conklin, and G. W. Pratt, Jr., Phys. Rev. Letters **11**, 538 (1963).
[2] F. Herman, K. F. Cuff, and R. L. Kortum, Phys. Rev. Letters **11**, 541 (1963).
[3] T. Loucks, Phys. Rev. Letters **14**, 1072 (1965).
[4] K. H. Johnson and H. Amar, Phys. Rev. **139**, A760 (1965); H. Amar, K. H. Johnson and K. P. Wang, *ibid.* **148**, 672 (1966); H. Amar and K. H. Johnson, *Optical Properties and Electronic Structure of Metals and Alloys* (North-Holland Publishing Co., Amsterdam, 1966); H. Amar, K. H. Johnson and C. B. Sommers, Phys. Rev. **153**, 655 (1967).
[5] W. Kohn and N. Rostoker, Phys. Rev. **94**, 1111 (1954).
[6] F. S. Ham and B. Segall, Phys. Rev. **124**, 1786 (1961).
[7] Y. Onodera, and M. Okasaki, J. Phys. Soc. Japan **21**, 1273 (1966).
[8] D. T. Cromer (private communication).
[9] P. O. Lowdin, Advan. Phys. **5**, 1 (1956).

which leads directly to the boundary condition

$$\frac{\partial\psi(r^c)}{\partial n^c}=-e^{i\mathbf{k}\cdot\mathbf{R}_0}\frac{\partial\psi(\tau)}{\partial n}, \tag{6}$$

where k is the wave vector of Eq. (4), r and r^c are conjugate points on the polyhedron surface, and R_0 is the translation vector joining points r and r^c (see KKR).

The boundary-value problem of Eqs. (4)–(6) can be solved using the Green's function $\mathcal{G}(r,r')$, which is the solution of the same boundary-value problem in which the right-hand side of Eq. (4) is replaced with the δ function $\delta(r-r')$. By means of the Green's function, this boundary-value problem is converted into an integral equation satisfied by the wave function and having as a kernel $K(r,r')=\mathcal{G}(r,r')V(r')$. KKR have shown that this integral equation can be directly obtained from the variational principle $\delta\Lambda=0$, where

$$\Lambda=\lim_{\epsilon\to0}\Lambda_\epsilon$$
$$=\lim_{\epsilon\to0}\int_{r<r_i-2\epsilon}d\tau\,\psi^*(r)V(r)$$
$$\times\left[\psi(r)-\int_{r'<r_i-\epsilon}d\tau'\,\mathcal{G}(r,r')V(r')\psi(r')\right], \tag{7}$$

where the limiting process required by the singularity of the Green's function is self-understood, and the integration is only over the region $r\leq r_m$ since the shifted potential $V(r)$ vanishes for $r>r_m$. Noting that the plane-wave solution $|s,k_n\rangle$ of the Dirac equation for a free particle is

$$(\boldsymbol{\alpha}\cdot\mathbf{p}+\beta)|s,k_n\rangle=k_n'|s,k_n\rangle, \tag{8}$$

the appropriate Green's function of Eq. (7) is

$$\mathcal{G}(r,r')=-\frac{1}{\tau}\sum_{n,s}\frac{\langle r|s,k_n\rangle\langle s,k_n|r'\rangle}{k_n'-W}, \tag{9a}$$

where τ is the volume of the polyhedron, and where

$$\mathbf{k}_n=\mathbf{k}+\mathbf{K}_n,\quad k_n'=(1+k_n^2)^{1/2},$$
$$\langle r|s,k_n\rangle=\left(\frac{1+k_n'}{2k_n'}\right)^{1/2}\begin{pmatrix}\chi(s)\\ [\boldsymbol{\sigma}\cdot\mathbf{k}_n/(1+k_n')]\chi(s)\end{pmatrix}e^{i\mathbf{k}_n\cdot\mathbf{r}}, \tag{9b}$$

and

$$\chi(s)=\begin{pmatrix}1\\0\end{pmatrix}\quad\text{or}\quad\begin{pmatrix}0\\1\end{pmatrix}$$

for $s=\pm\frac{1}{2}$, respectively. The Green's function of Eq. (7) satisfies the boundary conditions of Eqs. (3) and (5) and has the properties

$$\mathcal{G}(r-R_n,r')=e^{i\mathbf{k}_n\cdot\mathbf{R}_n}\mathcal{G}(r,r'),$$
$$\mathcal{G}(r,r')=\mathcal{G}^\dagger(r',r). \tag{10}$$

Within the muffin-tin sphere, the radial wave function is an eigenfunction of Dirac's central-field Hamiltonian. As a trial function in (7), we shall use the following:

$$|\psi(r)\rangle_k{}^\alpha=\sum_{K,\nu}i^{l_K}C_{K,\nu}{}^\alpha\begin{pmatrix}f_K(r)\\ ig_K(r)\delta_{K,-K}\end{pmatrix}\theta_{K,\nu}{}^\alpha, \tag{11}$$

where $\delta_{K,-K}$ means that we must replace K by $-K$ in

TABLE I. Energy eigenvalues in rydbergs at the various K (in units of $2\pi/a$) points of the face-centered zone. The notation used for the symmetry points is that of Elliot.

K	$E(K)$	K	$E(K)$
$\Gamma_6^+(0,0,0)$	−1.18	$\Delta_7(0.4,0,0)$	−0.795
			−0.545
			−0.645
$\Gamma_8^+(0,0,0)$	−0.58		
	−0.75		
		$\Delta_7(0.2,0,0)$	−0.77
			−0.665
			−0.57
$\Gamma_7^+(0,0,0)$	−0.67		
$\Delta_6(0.2,0,0)$	−1.11	$\Delta_7(0.6,0,0)$	−0.845
	−0.74		−0.57
	−0.59		−0.50
$\Delta_6(0.4,0,0)$	−1.0	$\Delta_7(0.8,0,0)$	−0.875
	−0.725		−0.53
	−0.62		−0.45
$\Delta_6(0.6,0,0)$	−0.96	$\chi_7^+(1,0,0)$	−0.89
	−0.68		−0.52
	−0.58		−0.42
			+0.2
$\Delta_6(0.8,0,0)$	−0.94	$\Sigma_8(0.125,0.125,0)$	−1.15
	−0.56		−0.765
	−0.485		−0.685
			−0.61
			−0.585
$\chi_6^+(1,0,0)$	−0.94		
	−0.51		
	−0.001	$\Sigma_8(0.250,0.250,0)$	−1.05
			−0.775
			−0.725
			−0.64
$\chi_6^-(1,0,0)$	−0.37		−0.555
$_8(0.5,0.5,0)$	−0.845	$\Lambda_{4^+,5^+}(0.375,0.375,0.375)$	−0.72
	−0.795		−0.52
	−0.74		
	−0.64		
	−0.58		
	−0.425	$\Lambda_{4^+,5^+}(0.250,0.250,0.250)$	−0.71
			−0.545
$K(0.75,0.75,0.75)$	−0.87		
	−0.835		
	−0.675		
	−0.54	$\Lambda_{4^+,5^+}(0.125,0.125,0.125)$	−0.73
	−0.49		−0.57
	−0.23		
$\Lambda_6(0.375,0.375,0.375)$	−0.97	$Q(5/8,3/8,4/8)$	−0.38
	−0.685		
	−0.67		
	−0.56		
		$W_7(1,0,0.5)$	−0.18
$\Lambda_6(0.125,0.125,0.125)$	−1.13		
	−0.76	$W_6(1,0,0.5)$	−0.16
	−0.67		
	−0.585		
$\Lambda_6(0.250,0.250,0.250)$	−0.97		
	−0.76		
	−0.64		
	−0.61		
$L_6^+(0.5,0.5,0.5)$	−0.94		
	−0.69		
	−0.52		
	−0.16		
$L_6^-(0.5,0.5,0.5)$	−0.54		
$L_{4^+,5^+}(0.5,0.5,0.5)$	−0.73		
	−0.43		

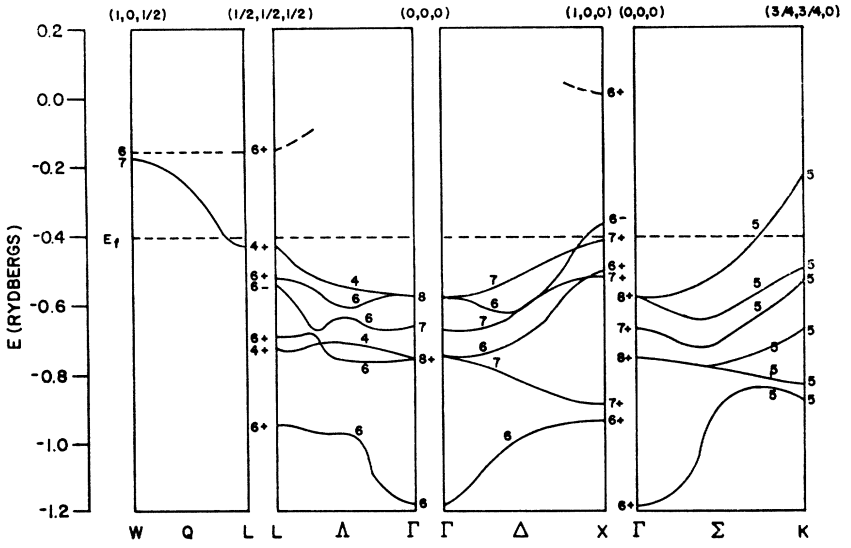

FIG. 1. Relativistic band structure of gold.

the Kubic harmonic factor $\theta_{K,\nu}{}^{\alpha}$, and where

$$\theta_{K,\nu}{}^{\alpha}=\sum_{\mu} a_{K',\mu}{}^{\alpha,\nu}\chi_{K',\mu} \tag{12}$$

is the basis function[10] of the αth irreducible representation.

The radial functions satisfy two coupled differential equations. The analysis from this point on follows the same pattern (variational principle, limiting process, etc.) as the KKR and Ham-Segall papers, with the appropriate relativistic adaptation. Details can be found in Onodera's paper[7] or in Sommers's doctoral dissertation.

The determination of the constant coefficients in (11) leads to a secular determinant, the zeros of which yield the energy values at a given **k** point, for a given irreducible representation of the symmetry group of that point.

A complete program was set up to perform these calculations on a CDC 6600. This program is available on request from the authors.

III. RESULTS AND DISCUSSION

The electronic band structure of gold was calculated at several points of high symmetry and at other general points of the fcc Brillouin zone. The resulting bands are shown in Fig. 1 and Table I. These bands may be compared with the nonrelativistic band structure which was computed by Schlosser[11] using the same choice of crystal potential but with an augmented-plane-wave method. The energies at several points of the zone were checked against Schlosser's and agreed with his results when the limit of $c\rightarrow\infty$ was taken in the relativistic program. This limit and the insertion of single group representations allows one to convert the relativistic program to the nonrelativistic one. A comparison of Fig. 1 with the nonrelativistic case showed that the bands in the relativistic case were shifted toward lower negative energies by about 0.22 Ry for the lowest-lying Γ states, to about 0.1 Ry for the d bands. These energies are given with respect to a shifted constant potential of $V_0=-1.082$ Ry in both cases. This downward shift is to be expected since the states of lower angular momentum should be affected to a greater extent. To see this, one transforms the Dirac equation by means of a double Foldy-Wouthuysen transformation and then notices that the mass-velocity and Darwin terms are largest when the electron is near the nucleus. For small r, the atomic orbitals go as r^l and are thus largest for the S-like states. Of course, in the crystal the electron wave functions are admixtures of different angular momentum states and thus the energy corrections will be symmetry-dependent.

The Fermi energy was determined by expanding the surface integral $\int k^3(\Omega,E_F)d\Omega$ in Kubic harmonics[12] and by interpolating this integral to the total number of conduction electrons. In this manner the Fermi level was found to lie at $E_F=-0.409$ Ry with respect to a constant potential $V_0=-1.082$ Ry.

The band structure of gold is more like that of copper than that of silver. In both copper and gold the width of the d bands is much wider, and the top of these bands is nearer the Fermi surface, than in silver (the gold d bands are even wider than the copper d bands).

A priori the Fermi surface is expected to be similar to that of Cu, i.e., to be formed of a "spherical belly" sprouting eight necks towards the hexagonal faces of the Brillouin zone. The specific geometric parameters of the Fermi surface of Au may be determined from our calculated band profiles. We have estimated the

[10] For a list of basis functions see Y. Onodera and M. Okazaki, J. Phys. Soc. Japan **21**, 2400 (1966).
[11] H. Schlosser (private communication).
[12] D. D. Betts, A. B. Bhatia, and M. Wyman, Phys. Rev. **104**, 37 (1956).

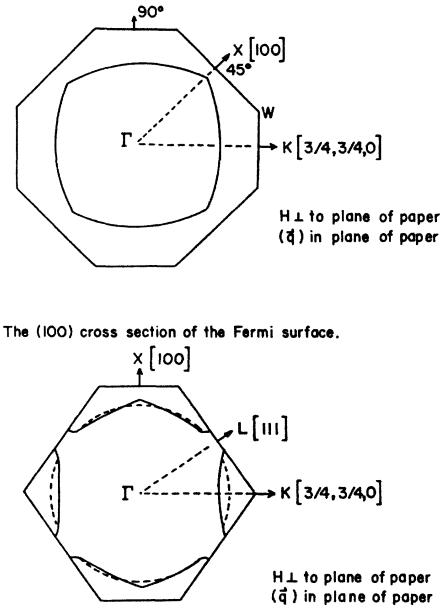

FIG. 2. Fermi-surface contours.

cross-sectional areas A_{100} of the belly and A_{111} of the neck. Table II provides a comparison between these calculated cross sections and those measured by Schoenberg[13] in his de Haas–van Alphen experiments of Au (The values listed are in units of 10^{16} cm^{-2}.) These cross-sectional areas are also shown in Fig. 2 (the area of the dotted circle is equivalent to the belly cross section).

Following Cooper, Ehrenreich, and Philipp,[14] we attempted to use the calculated energy bands to explain the optical absorption data of Beaglehole.[15]

[13] D. Schoenberg, Phil. Mag. **5**, 105 (1960).
[14] B. R. Cooper, H. Ehrenreich, and H. R. Philipp, Phys. Rev. **138**, A494 (1963).
[15] D. Beaglehole, *Optical Properties and Electronic Structure of Metals and Alloys* (John Wiley & Sons, Inc., New York, 1965), p. 154.

TABLE II. Comparison between our (110) and (111) cross-sectional areas and those measured by Schoenberg (the values listed are in units of 10^{16} cm^{-2}).

	Belly A_{110}	Neck A_{111}
Experiment	4.89	0.154
Theory	4.83	0.172
Free electron	4.5	none

According to these data, there are three peaks appearing in the imaginary part of the dielectric constant: at 3, 3.5, and 5 eV. Using the calculated bands, we could assign these peaks to three possible direct transitions: (1) transition Q_3 (near L_6^+) to Q_4 band which intersects the Fermi level, (2) transition X_7^+ to X_6^-, and (3) from K_5 right below the Fermi level to K_5 right above the Fermi level. However, the first two transitions are too small to account for the experimental results. Since there are no Van Hove critical points in the joint density of states in the K direction, one would expect the dipole transition probabilities to be much smaller in the K direction than in the X or L directions. Therefore, the third possibility is also unlikely. Thus, comparison with experimental data strongly suggests that the indirect transitions must play an important role.

In conclusion, while our calculated bands are in excellent agreement with the de Haas–van Alphen data and corroborate (at the limit $c \to \infty$) Schlosser's nonrelativistic calculations, they cannot provide a satisfactory interpretation of optical experiments if one confines oneself to the vertical-transition scheme of Cooper *et al.*[14] Appeal must be made to many-body effects and to phonon-assisted indirect transitions.

ACKNOWLEDGMENTS

We would like to thank D. Cromer for supplying us with the atomic charge densities, Y. Onodera for his tables of basis functions, and Dr. K. P. Wang for valuable discussions and suggestions.